Inorg. Chem. **2005**, *44*, 3087–3093

Synthesis, Crystal Structure, Magnetic Properties, and Electronic Structure of the New Ternary Vanadate $CuMnVO_4$

Hamdi Ben Yahia, Etienne Gaudin, and Jacques Darriet*

Institut de Chimie de la Matière Condensée de Bordeaux, 87 Avenue du Docteur Schweitzer, 33608 Pessac Cedex, France

Michael Banks and Reinhard K. Kremer*

Max-Planck-Institut für Festkörperforschung, Heisenbergstrasse 1, D-70569 Stuttgart, Germany

Antoine Villesuzanne† and Myung-Hwan Whangbo*

Department of Chemistry, North Carolina State University, Raleigh, North Carolina 27695-8204

Received December 14, 2004

A new magnetic oxide, $CuMnVO_4$, was prepared, and its crystal structure was determined by single-crystal X-ray diffraction. The magnetic properties of $CuMnVO_4$ were characterized by magnetic susceptibility and specific heat measurements, and the spin exchange interactions of $CuMnVO_4$ were analyzed on the basis of spin-polarized electronic band structure calculations. $CuMnVO_4$ contains MnO_4 chains made up of edge-sharing MnO_6 octahedra containing high-spin Mn^{2+} cations. Our work shows that $CuMnVO_4$ undergoes a three-dimensional antiferromagnetic transition at ~20 K. Both the intrachain and interchain spin exchanges are antiferromagnetic, and the interchain spin exchange is not negligible compared to the intrachain spin exchange.

1. Introduction

Recently it has been shown that lithium phosphates $LiMPO_4$ (M = transition metal) with the olivine structure, especially $LiFePO_4$,[1] are promising as high-potential cathode materials for rechargeable Li-ion batteries. Several olivine-type compounds were successfully tested as positive electrodes (e.g., $LiFePO_4$,[1,2] $LiMnPO_4$,[3] and $LiCoPO_4$[4]). The vanadate compounds $LiMVO_4$ crystallize with different structural types, i.e., the Na_2CrO_4-type structure for $LiMnVO_4$[5] and the spinel-type structure for $LiCoVO_4$, $LiNiVO_4$, and $LiCuVO_4$.[6,7] $LiMnVO_4$ is not a good positive electrode for lithium batteries,[5] while, as negative electrodes, the $LiMVO_4$ (M = Co, Ni, Cd, Zn) series possesses a high capacity at low voltage and delivers a lower output voltage than carbon-based batteries.[8] Compounds from the delithiated series, MVO_4 (M = In, Cr, Fe, Al, Y), were tested as negative electrodes, and $FeVO_4$ and $InVO_4$ were found to display a reversible capacity as high as 900 mAh g^{-1}.[9] So far, there have been no reports on either the existence of $MnVO_4$ or the test of $LiMnVO_4$ as a negative electrode.

The sharp distinction between $LiMnPO_4$ and $LiMnVO_4$ in their lithium intercalation properties is related to their structural differences. In $LiMnPO_4$, the lithium atoms form infinite LiO_4 chains made up of edge-sharing LiO_6 octahedra, and these chains are connected through sheets of corner-

* To whom correspondence should be addressed. E-mail: darriet@icmcb-bordeaux.cnrs.fr (J.D.); rekre@fkf.mpg.de (R.K.K.); mike_whangbo@ncsu.edu (M.-H.W.).

† Permanent address: ICMCB-CNRS, 87 Avenue du Docteur Schweitzer, 33608 Pessac Cedex, France.

(1) Pahdi, A. K.; Nanjundaswamy, K. S.; Goodenough, J. B. *J. Electrochem. Soc.* **1997**, *144*, 1188.
(2) Herle, P. S.; Ellis, B.; Coombs, N.; Nazar, L. F. *Nat. Mater.* **2004**, *3*, 147.
(3) Li, G. H.; Azuma, H.; Tohda, M. *Electrochem. Solid-State Lett.* **2002**, *5*, A135.
(4) Bramnik, N. N.; Bramnik, K. G.; Buhrmester, T.; Baehtz, C.; Ehrenberg, H.; Fuess, H. *J. Solid State Electrochem.* **2004**, *8*, 558.
(5) (a) Padhi, A. K.; Archibad, W. B.; Najundaswamy, K. S.; Goodenough, J. B. *J. Solid State Chem.* **1997**, *128*, 267. (b) Sato, M.; Kano, S.; Tamaki, S.; Misawa, M.; Shirakawa, Y.; Ohashi, M. *J. Mater. Chem.* **1996**, *6*, 1191.
(6) Gonzalez, C.; Gaitan, M.; Lopez, M. L.; Veiga, M. L.; Saez-Puche, R. *J. Mater. Sci.* **1994**, *29*, 3458.
(7) Kanno, R.; Kawamoto, Y.; Takeda, Y.; Hasegawa, M.; Yamamoto, O. *J. Solid State Chem.* **1992**, *96*, 397.
(8) Guyomard, D.; Sigala, C.; Le Gal La Salle, A.; Piffard, Y. *J. Power Sources* **1997**, *68*, 692.
(9) Denis, S.; Baudrin, E.; Touboul, M.; Tarascon, J.-M. *J. Electrochem. Soc.* **1997**, *144*, 4099.

10.1021/ic048244y CCC: $30.25
Published on Web 03/18/2005

sharing MnO_6 octahedra and PO_4 tetrahedra. The good reversible insertion of lithium in the olivine-type compounds is due to the LiO_4 chains which provide channels for the Li^+ ions to diffuse in and out. In $LiMnVO_4$, the infinite MnO_4 chains composed of edge-sharing MnO_6 octahedra are connected by VO_4 and LiO_4 tetrahedra, and the Li^+ ions are found in the double chains of alternating VO_4 and LiO_4 tetrahedra sharing edges and corners. The latter arrangement of polyhedra does not provide a channel through which Li^+ ions can diffuse.

Only a few lithium vanadate compounds with the Na_2CrO_4-type structure are observed, i.e., $LiMgVO_4$, $LiMnVO_4$, $LiCdVO_4$, and $Li_{0.9}(In_{0.6}Li_{0.3})VO_4$.[5,10−12] The fact that the Na_2CrO_4-type structures are not as numerous as the olivine-type structures can be attributed to the strong strain associated with the short distance between V^{5+} and Li^+ which results from the edge-sharing between the LiO_4 and VO_4 tetrahedra. One might speculate that substituting copper or sodium for the lithium in $LiMnVO_4$ may result in retention of that same structure, as found in $NaCdVO_4$ and $CuCdVO_4$.[13,14] Thus, we have attempted to synthesize the homologous compounds $NaMnVO_4$ and $CuMnVO_4$. Our attempt was successful only for $CuMnVO_4$ which is understandable in light of the compatibility of the cation sizes (0.99, 0.60, and 0.59 Å for the four-coordinate Na^+, Cu^+, and Li^+, respectively[15]).

In the present work, we first describe the synthesis and the crystal structure of $CuMnVO_4$ determined by single-crystal X-ray diffraction. We then describe the magnetic properties of $CuMnVO_4$ determined by magnetic susceptibility and heat capacity measurements. Finally, we discuss the structural and magnetic properties of $CuMnVO_4$ on the basis of electronic band structure calculations.

2. Experimental Section

$CuMnVO_4$ was prepared by a direct solid-state reaction of MnO, CuO, V_2O_5, and V_2O_3 in a 4:4:1:1 molar ratio. A redox reaction between V_2O_3 and CuO leads to the oxidation of vanadium from +3 to +5 and the reduction of Cu^{2+} to Cu^+ in the final product, $CuMnVO_4$.[14] The mixture was ground and fired at 750 °C in an argon atmosphere for 3 days with intermittent grinding. The latter procedure was repeated several times to obtain pure samples. Single crystals were prepared by heating the $CuMnVO_4$ powder at 950 °C for 12 h and cooling it very slowly (at 2 °C h^{-1}) to ambient temperature.

To ensure the homogeneity of the $CuMnVO_4$ sample, high-precision X-ray powder diffraction measurements were performed. The data were collected at room temperature over the 2θ angle range $5° \le 2\theta \le 120°$ with a step size of 0.02° using a Philips X-pert diffractometer operating with Cu Kα radiation. A full pattern matching refinement was performed with the JANA2000 program package.[16] The background was estimated by a Legendre function, and the peak shapes were described by a pseudo-Voigt function. The refinement of peak asymmetry was performed using four parameters.[17] Finally, a Rietveld refinement with the single-crystal atomic parameters allowed us to ensure the phase purity of the sample.

Table 1. Atom Position and Isotopic Displacement Parameters for $CuMnVO_4$[a]

atom	occupancy	site	x	y	z	U_{eq} (Å^2)
Cu	1	4c	0	0.32230(13)	3/4	0.0291(3)
Mn	1	4a	0	0	1/2	0.0094(2)
V	1	4c	0	0.64184(10)	3/4	0.0075(2)
O1	1	8g	0.2473(5)	0.4748(3)	1/4	0.0115(7)
O2	1	8f	0	0.2438(3)	0.4625(4)	0.0131(7)

[a] Crystal system = orthorhombic; space group = *Cmcm*; a = 5.787(2) Å, b = 8.807(3) Å, c = 6.410(2) Å; and Z = 4.

A crystal suitable for single-crystal X-ray diffraction was selected on the basis of the size and sharpness of the diffraction spots. The data collection was carried out on an Enraf-Nonius Kappa CCD diffractometer using Cu Kα radiation. Data processing and all refinements were performed with the JANA2000 program package. A Gaussian-type absorption correction was applied, and the shape was determined with the video microscope of the Kappa CCD. For data collection details, see Table S1 of the Supporting Information.

Magnetic susceptibility measurements were carried out with a Quantum Design SQUID magnetometer. The susceptibility was recorded at 5000 G where the magnetization is linear with the field in the whole temperature range (2−340 K). The diamagnetic corrections were carried out on the basis of Pascal's tables. Heat capacity measurements were performed using a quasi-adiabatic heat pulse method[18] (Nernst calorimeter). A powder sample of $CuCdVO_4$ (m = 1.88 g) was measured to provide a nonmagnetic reference to the magnetic $CuMnVO_4$ (m = 1.78 g). The powder samples were encapsulated in Duran glass ampules under ~1 bar of He gas to provide a thermal coupling. The glass ampules were attached with a minute amount of Apiezon vacuum grease to the sapphire sample platform. The heat capacity of the glass ampule, Apiezon, and sample holder was subtracted after measurement. The temperature range for the measurement was 4−250 K.

3. Crystal Structure

The extinction conditions observed for $CuMnVO_4$ agree with the *Cmcm* space group already used for the refinement of the homologous compound $LiMnVO_4$.[5] The starting atomic positions were those reported for $LiMnVO_4$. With anisotropic displacement parameters, the final residual factors converged to the value $R(F) = 0.0356$ and $wR(F^2) = 0.1091$ for 25 refined parameters and 433 observed reflections (Table 1). The refined atomic positions and anisotropic displacement parameters (ADPs) are given in Table 1 and Table S2, respectively. The U^{11} component for copper has a large value (i.e., 0.047 Å^2) which may indicate disorder in the copper position. However, the difference Fourier maps showed no splitting of the copper position. Thus, the copper Debye−Waller factor up to the fourth order was tested by means of a Gram−Charlier expansion. This reduced the reliability

(10) Barbier, J. *Eur. J. Solid State Inorg. Chem.* **1988**, *25*, 609.
(11) Ben Amara, M. Ph.D. Thesis, Université de Bordeaux 1, Talence Cedex, France, 1979.
(12) Touboul, M.; Toledano, P. *J. Solid State Chem.* **1981**, *38*, 386.
(13) Le Flem, G.; Olazcuaga, R. *Bull. Soc. Chim. Fr.* **1968**, *7*, 2769.
(14) Feldmann, J.; Muenchau, S.; Mueller-Buschbaum, H. *Z. Naturforsch. B* **1995**, *50b*, 871.
(15) Shannon, R. D. *Acta Crystallogr. A* **1976**, *32*, 751.
(16) Petricek, V.; Dusek, M. *The Crystallographic Computing System Jana*; Institute of Physics: Praha, Czech Republic, 2000.
(17) Berar, J. F.; Baldinozzi, G. *J. Appl. Crystallogr.* **1993**, *26*, 128.
(18) Schnelle, W.; Gmelin, E. *Thermochim. Acta* **2002**, *391*, 41.

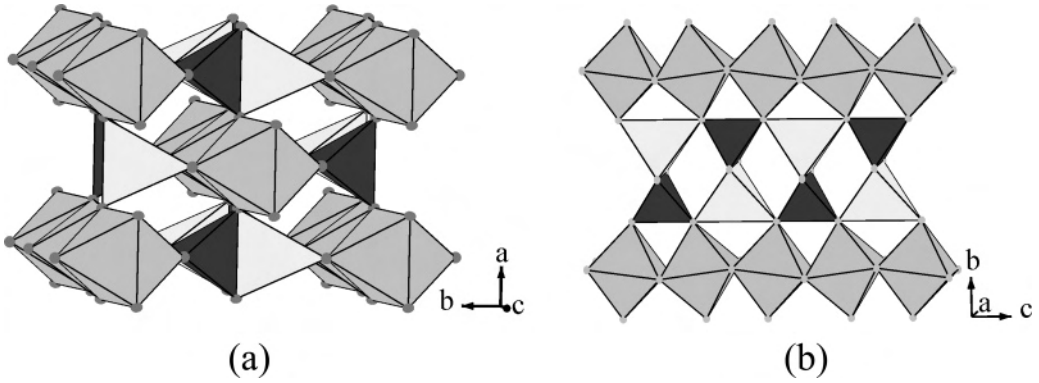

Figure 1. Perspective polyhedral views of the crystal structure of $CuMnVO_4$ approximately (a) along the *c*-direction and (b) along the *a*-direction. The gray octahedra represent the MnO_6 octahedra, the small dark tetrahedra the VO_4 tetrahedra, and the large light tetrahedra the CuO_4 tetrahedra.

Table 2. Interatomic Distances (in Å) and Angles (in deg) for $CuMnVO_4$

distances		angles	
Cu−O1 (×2)	2.289(3)	O1−Mn−O1	84.23(8)
Cu−O2 (×2)	1.969(3)	O1−Mn−O2	88.90(9)
Mn−O1 (×4)	2.181(2)	O1−Cu−O1	77.39(11)
Mn−O2 (×2)	2.160(3)	O1−Cu−O2	105.92(7)
V−O1 (×2)	1.762(3)	O2−Cu−O2	138.85(14)
V−O2 (×2)	1.694(3)	O1−V−O1	108.63(14)
Cu···V	2.8142(15)	O1−V−O2	110.30(7)
		O2−V−O2	107.02(15)

factors to $R(F) = 0.0309$ and $wR(F^2) = 0.0915$ for 34 refined parameters with difference Fourier residues in the range between −1.06 and +1.31 eÅ^{-3}. Analysis of the probability density function of copper for both refinements does not show a significant difference so the classical model with ADPs for all positions was kept.

The crystal structure of $CuMnVO_4$ is characterized by MnO_4 chains made up of edge-sharing MnO_6 octahedra which are parallel to the *c*-direction (Figure 1). The VO_4 and CuO_4 tetrahedra share an edge along the *a*-direction to form $CuVO_6$ dimers which share corners to form $CuVO_4$ double chains parallel to the *c*-direction. The $CuVO_4$ double chains and the MnO_4 octahedral chains are condensed together by corner-sharing. The interatomic distances for the MnO_6, VO_4, and CuO_4 polyhedra are listed in Table 2. The average distances of the Mn−O, V−O, and Cu−O bonds are 2.174, 1.729, and 2.121 Å, respectively, and are very close to the values estimated from the effective ionic radii of Mn^{2+}, V^{5+}, Cu^+, and O^{2-}.[15] Moreover, the calculations of the bond valence sum (BVS) confirm this charge balance (i.e., BVS = 2.13, 4.92, and 1.08 for Mn^{2+}, V^{5+}, and Cu^+, respectively).[19]

The edge-sharing between regular CuO_4 and VO_4 tetrahedra leads to a short Cu^+−V^{5+} distance. Thus, in each $CuVO_6$ dimer of $CuMnVO_4$, the Cu^+ and V^{5+} ions are displaced toward the outside edges of the tetrahedron resulting in a realistic Cu^+−V^{5+} distance of 2.814 Å (Figure 2). As shown in Table 2, the displacement of the Cu^+ ion from the tetrahedron center is twice as large as the one for the V^{5+} ion. Such disproportionate cation displacements have also been found for $LiMnVO_4$,[5] $CuCdVO_4$, and $[Li_{1/3}Cd_{1/3}\square_{1/3}]$-$CdVO_4$.[14,20] The reason that the shifts of the Cu^+ and Li^+ ions are large while the V^{5+} ion remains close to the tetrahedron center in these compounds is discussed later (see section 5.1).

(19) Brown, I. D.; Altermatt, D. *Acta Crystallogr. B* **1985**, *41*, 244.

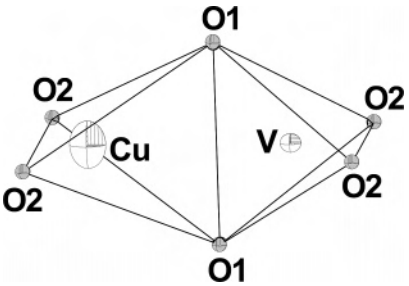

Figure 2. Perspective view of the $CuVO_6$ dimer of $CuMnVO_4$.

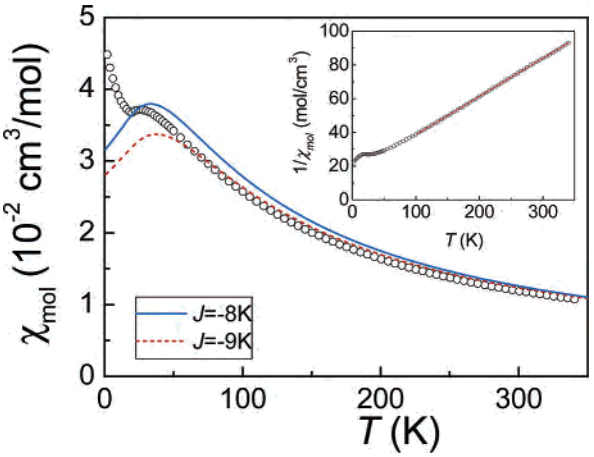

Figure 3. Magnetic susceptibility of $CuMnVO_4$ (○) and calculated susceptibility for a classical Heisenberg chain ($S = 5/2$) with the exchange constants equal to −8 K (blue solid curve) and −9 K (red dashed curve). The inset displays the reciprocal susceptibility with a Curie−Weiss fit (red solid line) indicating a paramagnetic Curie temperature of −70(1) K (see the text for other parameters).

4. Magnetic Susceptibility and Heat Capacity

The magnetic susceptibility χ vs T for $CuMnVO_4$ is presented in Figure 3, and the corresponding χ^{-1} vs T plot is given in the inset. The χ^{-1} vs T plot reveals that $CuMnVO_4$ exhibits a paramagnetic behavior in the temperature range 100−340 K. The susceptibility above 150 K follows a

(20) Gaudin, E.; Ben Yahia, H.; Shikano, M.; Ben Amara, M.; zur Loye, H. C.; Darriet, J. *Z. Kristallogr.* **2004**, *219*, 755.

Curie−Weiss law with $\theta = -70(1)$ K and $C = 4.41$ mol^{-1} cm^3 K which indicates a predominant antiferromagnetic interaction between adjacent Mn^{2+} ions. The effective magnetic moment μ_{eff} calculated from the Curie constant is 5.94(1) μ_B which is in good agreement with the spin-only value of 5.92 μ_B expected for a high-spin Mn^{2+} (d^5) ion. In the mean field approximation, the paramagnetic Curie−Weiss temperature, θ, is given by[21]

$$\theta = \frac{zS(S+1)}{3}\frac{J}{k_B} \quad (1)$$

where $S = 5/2$ for the high-spin Mn^{2+}, J is the spin exchange parameter between two adjacent magnetic sites, and z is the number of nearest-neighbor magnetic sites around a given magnetic site. (Here we use the convention in which the spin exchange Hamiltonian between two spin sites i and j is written as $-J_{ij}\hat{S}_i\hat{S}_j$.) If it is assumed that the interactions of $CuMnVO_4$ are dominated by the intrachain spin exchange, J_{intra}, of its MnO_4 chains, then $z = 2$. With $\theta = -70(1)$ K, $z = 2$, and $S = 5/2$, we obtain $J_{intra}/k_B \approx -12$ K from eq 1.

The susceptibility shows a local maximum at ~25 K and a local minimum at ~20 K followed by an increase toward low temperatures. If we assume predominant antiferromagnetic intrachain exchange, the magnetic susceptibility can be described by a Heisenberg chain model. The magnetic susceptibility of a classical Heisenberg chain with spin S and intrachain exchange J_{intra} is given by

$$\chi_{CH} = \left(\frac{C}{T}\right)\frac{1+u(T)}{1-u(T)} \quad (2)$$

with $u(T) = \coth K - 1/K$, $K = J_{intra}S(S+1)/k_BT$, and the Curie constant $C = Ng^2\mu_B{}^2S(S+1)/3k_B$.[22,23] Figure 3 shows a comparison of eq 2 in which J_{intra}/k_B is assumed to be −8 and −9 K with the experimentally determined susceptibility of $CuMnVO_4$. The deviations are significant which indicates that a simple chain model is not adequate to properly describe the magnetic behavior. We must assume that a significant interchain exchange, which may eventually lead to a long-range magnetic ordering at certain temperatures, exists.

To confirm the above speculation, we carried out heat capacity measurements for $CuMnVO_4$ between 4 and 250 K. The specific heat of the isostructural compound $CuCdVO_4$ was also measured as the reference for its nonmagnetic lattice. As shown in Figure 4, the specific heat of $CuMnVO_4$ exhibits a λ-type anomaly at 19.3(3) K. Therefore, the local minimum in the χ vs T plot is associated with a 3D antiferromagnetic phase transition. The specific heat of $CuCdVO_4$ is featureless because it has no magnetic ions.

The magnetic contributions to the specific heat $C_m(T)$ of $CuMnVO_4$ may be approximated by the specific heat of $CuMnVO_4$ minus that of $CuCdVO_4$. In this process the heat capacity of $CuCdVO_4$ should be reduced (by a factor of ~0.93) so that the heat capacity of $CuMnVO_4$ and $CuCdVO_4$ match at high temperatures ($T > 80-100$ K) where magnetic contributions are expected to be negligible. This procedure may lead to some errors if the heat capacity of $CuMnVO_4$ has contributions from extended short-range magnetic ordering, which are difficult to estimate because the lattice heat capacity dominates the total heat capacity at high temperatures. Furthermore, since the mass of Cd is about twice that of Mn, the acoustic phonon spectra of $CuMnVO_4$ and $CuCdVO_4$ may be different so that the heat capacity of $CuCdVO_4$ may not represent an adequate lattice reference at low temperatures. The magnetic entropy obtained by integrating the $C_m(T)/T$ curve shows that the total magnetic entropy of $CuMnVO_4$ per formula unit is lower than the expected value, $R\ln(2S+1) = R\ln 6$, by approximately 30%. This agreement is acceptable in light of the aforementioned problems in constructing the lattice reference heat capacity.

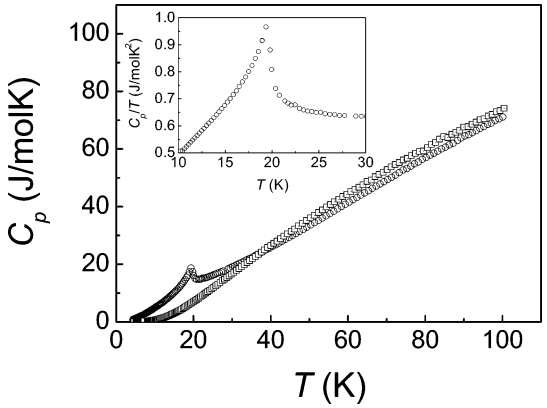

Figure 4. Heat capacities, $C_p(T)$, of $CuMnVO_4$ (○) and its nonmagnetic reference $CuCdVO_4$ (□). The inset displays C_p/T in the region of the phase transition at 19.3(5) K.

In view of the sizable interchain coupling indicated by the Néel temperature, 19.3 K, we fitted the magnetic susceptibility with an interchain exchange modified susceptibility which takes into account the interchain interaction characterized by the interchain paramagnetic Curie temperature, θ_{inter}. To have a reasonable estimate of θ_{inter} from the observed magnetic susceptibility, it is necessary to remove the contribution $x_{imp}C/T$ from a Curie-type impurity. Thus, the observed susceptibility can be fitted by the modified susceptibility $\chi'(T)$ written as

$$\chi'(T) = (1-x_{imp})\frac{\chi_{CH}(T)}{1-\theta_{inter}\left[\frac{\chi_{CH}(T)}{C}\right]} + x_{imp}C/T \quad (3)$$

where $\chi_{CH}(T)$ is given by eq 2. By analogy to eq 1, θ_{inter} gives the interchain exchange coupling, J_{inter}, with $z_{inter} = 4$. The amount of impurities is characterized by x_{imp}; we ascribe $S = 5/2$ free moments with the Curie constant $C = 4.38$ cm^3 K mol^{-1}. Using eq 3, we fitted the magnetic susceptibility in the temperature regime above $T_N = 19.3$ K and obtained a very good agreement (Figure 5) with $x_{imp} = 0.01$, $\theta_{inter} = -22(1)$ K, $J_{inter}/k_B = -2$ K, and $J_{intra}/k_B = -7.0(3)$

(21) Kahn, O. *Molecular Magnetism*; VCH: New York, 1993.
(22) Fisher, M. E. *Am. J. Phys.* **1964**, *32*, 343.
(23) Carlin, R. L. *Magnetochemistry*; Springer-Verlag: Berlin, 1986; p 170.

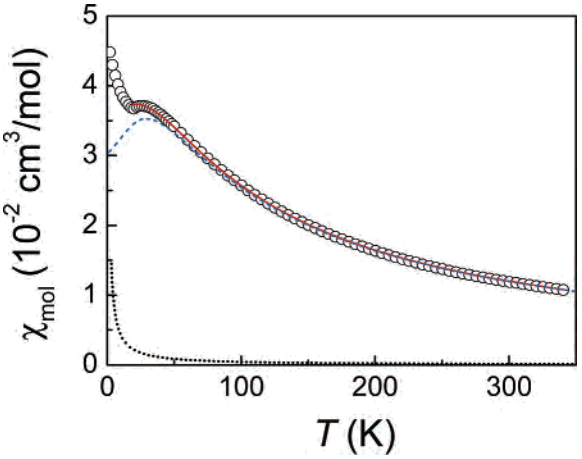

Figure 5. Experimental magnetic susceptibility of CuMnVO4 (○) and calculated interchain exchange corrected susceptibility according to eq 3 (red solid line). Only the data between ~20 and 340 K were fitted. The blue dashed curve represents the contribution of the interchain exchange corrected classical Heisenberg chain susceptibility alone. The black dotted curve shows the Curie-type susceptibility of ~1% of free $S = 5/2$ moments, which was added to account for traces of impurities responsible for the sharp susceptibility upturn below the three-dimensional antiferromagnetic transition at ~20 K.

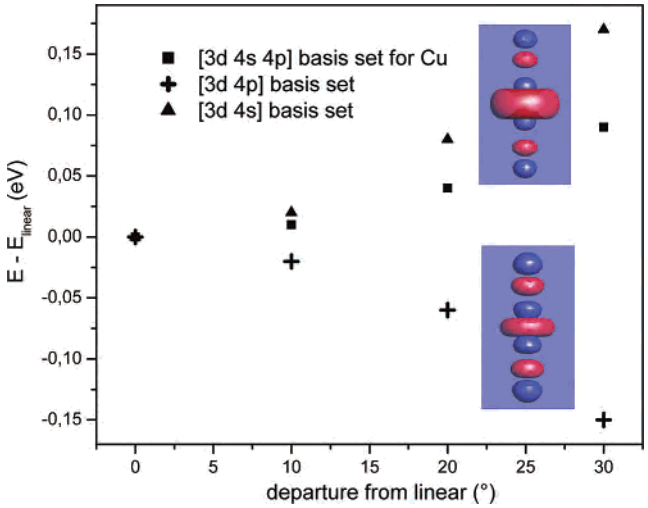

Figure 6. Relative energy of a $[O-Cu-O]^{3-}$ unit as a function of the O−Cu−O angle, for three valence basis sets, calculated with the extended Hückel tight-binding method. The top and bottom insets show the $3d_{z^2}$-block orbitals calculated with and without the Cu 4s orbital, respectively.

K. Thus, the interchain exchange is weaker than the intrachain spin exchange by a factor of approximately 3. As an additional consistency check, we compared the paramagnetic Curie temperature, θ, obtained from the fit of the high-temperature reciprocal susceptibility with the high-temperature expansion of eq 3 without the impurity contribution. The latter gives

$$\chi' = \frac{C}{T - (\theta_{intra} + \theta_{inter})} \tag{4}$$

which implies that $\theta = \theta_{intra} + \theta_{inter}$. With $z_{intra} = 2$, $z_{inter} = 4$, $J_{intra}/k_B = -7$ K, and $J_{inter}/k_B = -2$ K, θ is calculated to be −64 K according to eq 1. This is in good agreement with the value, −70 K, deduced from the fit of the high-temperature reciprocal susceptibility.

5. Electronic Structure Analysis

5.1. Metal Atom Displacement from the MO_4 (M = Cu, Li, V) Tetrahedral Center. As described in section 3, the shifts of the Cu^+ and Li^+ ions from the MO_4 (M = Cu, Li) tetrahedral centers are large, whereas the V^{5+} ion remains close to the VO_4 tetrahedral center. The VO_4 tetrahedron is much smaller than the CuO_4 or LiO_4 tetrahedron (Figure 1, Table 2) because of the smaller ionic radius and higher net charge for V^{5+} than for Cu^+ and Li^+. Moreover, from the viewpoint of the ionic electron counting scheme, all the d orbitals of a V^{5+} ion are empty. In each VO_4 tetrahedron, the empty d orbitals give rise to covalent interactions with the p orbitals of the surrounding four O^{2-} anions. The maximum stabilization from these interactions occurs when the V^{5+} ion can interact equally with all four O^{2-} anions, i.e., when the V^{5+} ion is at the center of each VO_4 tetrahedron.

Compared with the V^{5+} ion, the Cu^+ and Li^+ ions occupy larger sites, are much less charged, and form less covalent bonds with oxygen. Therefore, their displacement from the tetrahedron center is greatly facilitated. The 3d/4s hybridization of Cu^+, which greatly favors the linear coordination (as discussed extensively in earlier studies[24]), contributes to the Cu displacement in $CuMnVO_4$. In the HOMO of a linear O−Cu−O entity, the orbital character of Cu is given by the $3d_{z^2}$/4s hybrid orbital which reduces the antibonding interaction with the oxygen 2p orbital (the inset of Figure 6). This makes the linear coordination of Cu^+ energetically favorable. Figure 6 shows the energy of a $[O-Cu-O]^{3-}$ unit calculated as a function of the ∠O−Cu−O angle using the extended Hückel tight-binding method.[25,26] It is noted that linear coordination is no longer favorable for Cu^+ when the 4s orbital is removed from the basis set. However, in the case of Li^+,no hybridization favoring linear coordination occurs; the crystal structure of Li_2O[27] is made up of regular LiO_4 tetrahedra, as opposed to the linear coordination of Cu^+ in the crystal structure of Cu_2O.[28]

5.2. Spin Exchange Interaction. To examine the spin exchange interactions of $CuMnVO_4$, first principles density functional theory (DFT) electronic structure calculations were performed using the full-potential all-electrons (linearized)-augmented plane wave + local orbitals (L/APW+lo) method[29,30] as implemented in the WIEN2k code.[31] The generalized gradient approximation in the formulation of Perdew, Burke, and Ernzherof[32] was used for the exchange

(24) Gaudin, E.; Boucher, F.; Evain, M. *J. Solid State Chem.* **2001**, *160*, 212.
(25) Hoffmann, R. *J. Chem. Phys.* **1963**, *39*, 1397.
(26) Our calculations were carried out using the *SAMOA* (Structure and Molecular Orbital Analyzer) program package (Dai, D.; Ren, J.; Liang, W.; Whangbo, M.-H. http://chvamw.chem.ncsu.edu/, 2002).
(27) Zintl, E.; Harder, A.; Dauth, B. *Z. Elektrochem.* **1934**, *40*, 588.
(28) Kirfel, A.; Eichhorn, K. D. *Acta Crystallogr. A* **1990**, *46*, 271.
(29) Sjöstedt, E.; Nordström, L.; Singh, D. *Solid State Commun.* **2000**, *114*, 15.
(30) Madsen, G. K. H.; Blaha, P.; Schwarz, K.; Sjöstedt, E.; Nordström, L. *Phys. Rev. B* **2001**, *64*, 195134.
(31) Blaha, P.; Schwarz, K.; Madsen, G. K. H.; Kvasnicka, D.; Luitz, J. *WIEN2k, An Augmented Plane Wave Plus Local Orbitals Program for Calculating Crystal Properties*; Vienna University of Technology: Vienna, Austria, 2001.

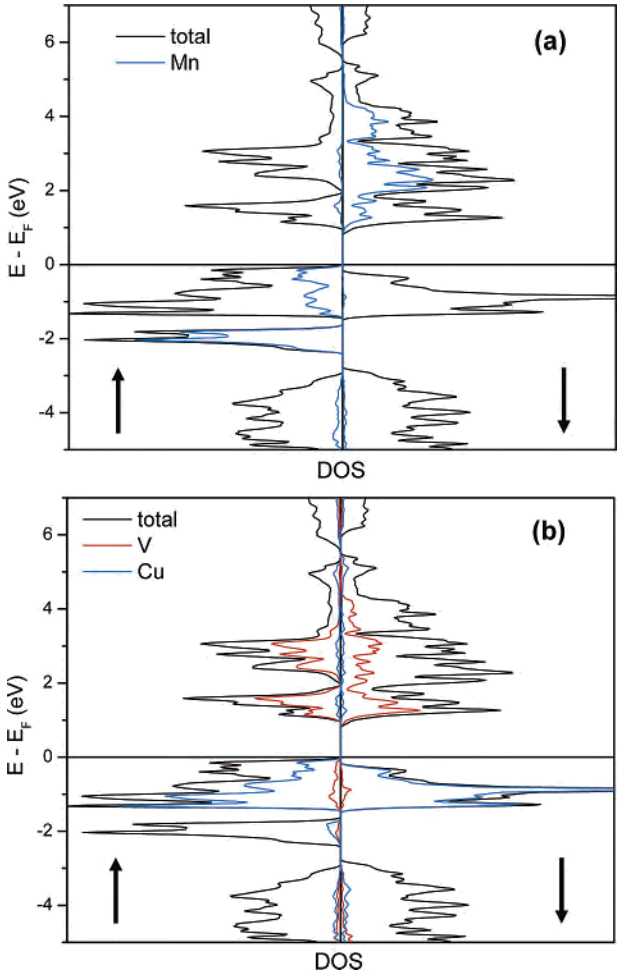

Figure 7. DOS plots calculated for the FM state of $CuMnVO_4$. (a) Total DOS vs partial DOS for Mn. (b) Total DOS vs partial DOS for V and Cu.

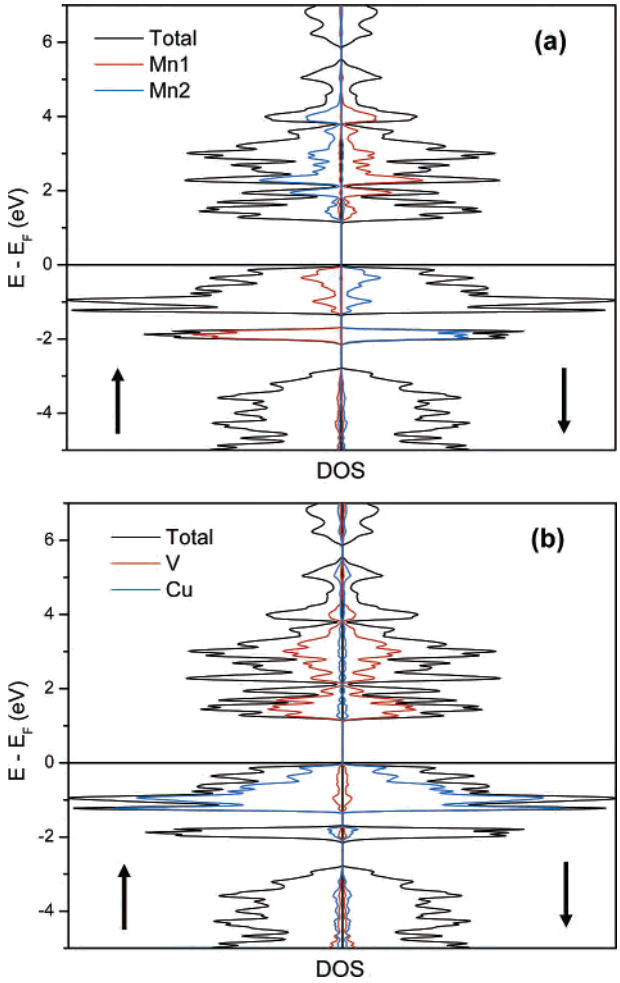

Figure 8. DOS plots for the AFM2 state of $CuMnVO_4$. (a) Total DOS vs partial DOS for Mn. (b) Total DOS vs partial DOS for V and Cu.

correlation potential. Atomic sphere radii were 2.1 au for Mn and Cu, 1.7 au for V, and 1.5 au for O. The Brillouin zone was sampled by 250 k-points. The plane-wave cutoff was $R_{MT}K_{max} = 7$. The energy criterion for self-consistency was set to less than 1 meV per FU.

Three ordered spin states were considered for our calculations. In the ferromagnetic state (FM), the spins in each MnO_4 chain and between adjacent MnO_4 chains are ferromagnetically ordered. In the first antiferromagnetic state (AFM1), the spins in each MnO_4 chain are antiferromagnetically ordered, but the spins between adjacent MnO_4 chains are ferromagnetically ordered. In the second antiferromagnetic case (AFM2), the spins are antiferromagnetically coupled within each chain and between adjacent chains. The AFM2 spin arrangement represents a 3D antiferromagnetic ordering. In the AFM1 and AFM2 states, the crystal symmetry was lowered to *Pmcm* and *Pmnn*, respectively, because of the occurrence of nonequivalent Mn sites.

In agreement with our experimental findings, the relative energies of the three ordered spin states increase in the order AFM2 < AFM1 < FM. Per FU, the AFM1 state is more stable than the FM state by 25 meV, while the AFM2 state is more stable than the AFM1 state by 6 meV. Figures 7 and 8 show the density of state (DOS) plots calculated for the FM and AFM2 states. The partial DOS (PDOS) plots calculated for Mn (Figures 7a and 8a) indicate that the Mn^{2+} ion has a high-spin d^5 configuration, and this is confirmed by the calculated total spin moment per FU (Table 3). The PDOS plots calculated for Cu and V (Figures 7b and 8b) show that their formal oxidation states are Cu^+ (d^{10}) and V^{5+} (d^0), respectively. Note from the PDOS plots for Cu and Mn that the half-filled d-block bands of Mn^{2+} lie lower than the completely filled d-block bands of Cu. A small spin moment found for V (Table 3) comes from the contribution of the V orbitals to the Cu-block bands, not from a partial filling of the V-block bands. In the AFM2 state, the spin moments are located primarily on the Mn sites and are antiferromagnetically ordered along the *c*-, (*a* + *b*)-, and (*a* − *b*)-directions.

Table 3. Unpaired Spin Densities Calculated for the FM and AFM2 States of $CuMnVO_4$ Using the L/APW+lo Method

	Mn	V	Cu	O	interstitial	total
FM	4.26	0.21	<0.03	<0.03	0.40	5.0
AFM2	±4.24	$<10^{-2}$	$<10^{-2}$	<0.02	$<10^{-2}$	0

Spin exchange interactions of a solid composed of magnetic ions with *N* unpaired spins may be described by

(32) Perdew, J. P.; Burke, K.; Ernzerhof, M. *Phys. Rev. Lett.* **1996**, *77*, 3865.

an Ising Hamiltonian.[33−35] The spin exchange interactions of $CuMnVO_4$ can be described in terms of the two exchange parameters, J_{intra} and J_{inter}, which are the nearest-neighbor spin exchange parameters within and between the chains, respectively. Then, per FU, the total spin exchange interaction energies of the FM, AFM1, and AFM2 states are written as

$$E_{FM} = (N^2/4)(-J_{intra} - 2J_{inter})$$
$$E_{AMF1} = (N^2/4)(J_{intra} - 2J_{inter})$$
$$E_{AMF2} = (N^2/4)(J_{intra} + 2J_{inter}) \quad (5)$$

where $N = 5$ for $CuMnVO_4$. Therefore, the J_{intra} and J_{inter} parameters can be related to the energy differences between the ordered spin states as

$$J_{intra} = (2/N^2)(E_{AMF1} - E_{FM})$$
$$J_{inter} = (1/N^2)(E_{AMF2} - E_{AMF1}) \quad (6)$$

Thus, given the calculated energy differences of $E_{AMF1} - E_{FM} = -25$ meV and $E_{AMF2} - E_{AMF1} = -6$ meV per FU, we obtain $J_{intra}/k_B = -23$ K and $J_{inter}/k_B = -2.8$ K. The calculated J_{intra} is greater than the value deduced from the susceptibility fitting by a factor of 3. Such a discrepancy is not surprising because DFT calculations tend to overestimate the magnitude of spin exchange interactions by a factor of up to four.[34,36,37] The calculated J_{inter}/J_{intra} ratio is approximately 1/10, which is somewhat smaller than the 1/3 ratio deduced from the susceptibility fitting. In any event, the results of our calculations are consistent with those of our susceptibility fitting analysis in that both the intrachain and the interchain spin exchange interactions are antiferromagnetic and the interchain spin exchange is not negligible.

6. Concluding Remarks

The magnetic oxide $CuMnVO_4$ prepared in our work contains MnO_4 chains made up of edge-sharing MnO_6 octahedra containing high-spin Mn^{2+} cations. The specific heat measurements show that $CuMnVO_4$ undergoes a three-dimensional antiferromagnetic transition at ∼20 K. In agreement with this finding, both the fitting analysis of the magnetic susceptibility and the electronic band structure calculations show that the intrachain and interchain spin exchanges are antiferromagnetic and the interchain spin exchange is not negligible when compared with the intrachain spin exchange.

Acknowledgment. The work at North Carolina State University was supported by the Office of Basic Energy Sciences, Division of Materials Sciences, U.S. Department of Energy, under Grant DE-FG02-86ER45259. The authors thank the Pole M3PEC, Bordeaux 1 University, for computing resources. We thank M. Ahrens for experimental assistance.

Supporting Information Available: Crystallographic data in CIF format. Table S1 is the crystallographic data and parameters of data collection and structure refinements of $CuMnVO_4$, and Table S2 is the anisotropic displacement factors for $CuMnVO_4$. This material is available free of charge via the Internet at http://pubs.acs.org.

IC048244Y

(33) Whangbo, M.-H.; Koo, H.-J.; Dai, D. *J. Solid State Chem.* **2003**, *176*, 417 and references therein.
(34) Dai, D.; Whangbo, M.-H. *J. Chem. Phys.* **2001**, *114*, 2887.
(35) Dai, D.; Whangbo, M.-H. *J. Chem. Phys.* **2003**, *118*, 29.
(36) Dai, D.; Koo, H.-J.; Whangbo, M.-H. *J. Solid State Chem.* **2003**, *175*, 341.
(37) Grau-Crespo, R.; de Leeuw, N. H.; Catlow, C. R. *J. Mater. Chem.* **2003**, *13*, 2848.